Unravelling the potential of fibrous silica zirconia catalyst for CO methanation in energy production

Abdul Hakim Hatta[1], *Norafneeza* Norazahar[1,2*], *Muhammad Akmal* Aziz[1], and *Mansur* Alhassan[1]

[1]Faculty of Chemical and Energy Engineering, Universiti Teknologi Malaysia, 81310 UTM Johor Bahru, Johor, Malaysia
[2]Centre of Hydrogen Energy, Institute of Future Energy, 81310 UTM Johor Bahru, Johor, Malaysia

Abstract. In this contemporary era of rapid progress, the global demand for energy has reached unprecedented levels, placing considerable strain on existing energy supplies. To address this challenge, synthetic or substituted natural gas (SNG) has emerged as a groundbreaking energy source attained through the methanation reaction of hydrogen and carbon monoxide (CO). This paper unveils a successful synthesis method for fibrous silica zirconia (FSZr) exploiting the microemulsion procedure, subsequently applied in the CO methanation process. The catalyst underwent comprehensive characterization using advanced techniques, including Fourier Transform Infrared (FTIR) spectroscopy, Field-Emission Scanning Electron Microscopy (FESEM), x-ray diffraction (XRD), and N_2 adsorption-desorption. The experimental results clearly demonstrate the exceptional catalytic performance of FSZr when compared to commercially available ZrO_2. At a temperature of 500 ºC, FSZr achieved a CO conversion and CH_4 yield of 20.76% and 11.52%, respectively. The remarkable achievements are credited to FSZr's distinct fibrous structure, expansive surface area, and exceptional basic characteristics. The heightened surface area facilitates better access to reactive sites, while the strong basic properties enable easier adsorption of the reactant. These combined factors significantly enhanced the effectiveness of the CO methanation procedure. These findings underscore the significance of fibrous morphology in zirconia catalysts for CO methanation, presenting a promising avenue for further research and insights into meeting the global energy demands efficiently.

1 Introduction

Ever since the groundbreaking work of Sabatier and Senderens unveiled the formation of methane through the interaction of hydrogen and carbon oxide, the methanation process has been subjected to thorough exploration [1, 2]. Its significance resonates deeply in the realm of chemical manufacturing, encompassing crucial functions such as purging CO_x remnants from hydrogen-rich feed gases, enhancing the quality of reformate gas for employment in fuel cells, and facilitating the creation of substitute energy reservoirs, exemplified by substitute natural gas (SNG) [3, 4]. In the realm of economic viability, SNG has the potential to be generated and circulated using the current pipeline network. Moreover, the growing demand for natural gas has elevated its status as a notably eco-friendly fuel compared to its fossil fuel counterparts, boasting significantly superior environmental benefits. Notably, natural gas has undergone a decline in cost, enhancing its attractiveness from a financial standpoint in recent times, marking a commendable stride forward [5]. Owing to its mineral-free composition, natural gas exhibits a cleaner combustion profile compared to air, avoiding the formation of ash residues upon burning. This intrinsic property positions it as an environmentally superior fuel in contrast to coal. Moreover, methane, a key component of natural gas, serves as an exemplary energy transporter, boasting an exceptional calorific potency at 55.7 kJ g^{-1}. This figure significantly surpasses the energy densities offered by petroleum (43.6 kJ g^{-1}) and coal (39.3 kJ g^{-1}), underscoring its prominence as a high-caliber energy resource [6, 7]. Therefore, it becomes evident that natural gas holds the capacity to excel beyond coal and other liquid fuels, the latter of which tend to harbor elevated levels of carbon content. This distinctive attribute underscores the heightened environmental and efficiency advantages associated with natural gas as an energy source [6]. The CO methanation process stands as a highly effective mechanism for generating methane, a fundamental constituent of natural gas. Due to the markedly exothermic nature of this process, the integration of a catalyst typically becomes imperative to lower the activation energy required. Incorporating a catalyst into this reaction has the capacity to significantly accelerate the pace at which CO gets transformed into methane. Extensive research endeavours have been undertaken to delineate the precise selectivity and reaction rates exhibited by n[1]umerous metallic elements and their corresponding support materials [8]. Despite these endeavours, a cluster of critical challenges tied to CO methanation necessitates further investigation. The deactivation of catalysts due to coking and sintering represents a substantial hurdle, notably impeding the practical application of these catalysts, particularly those of metallic nature [9]. This issue warrants comprehensive

*Corresponding author: norafneeza@utm.my

exploration to unlock the full potential of CO methanation as a process.

In the modern era, ZrO_2 has arisen as one of the outstanding transition metal oxides within the realm of heterogeneous catalysts. This ascent can be attributed to the distinctive attributes exhibited by this material, including heightened reactivity, exceptional thermal robustness, sustained stability, and limited carbon deposition. These attributes arise from the plentiful availability of active sites and oxygen vacancies inherent to the catalyst [10-13]. The ongoing pursuit of research has been directed towards augmenting the activity of ZrO_2 even further, utilizing novel approaches for catalyst fabrication and introducing supplementary promoters. Despite these efforts, there remains a critical need for more extensive investigations aimed at amplifying the catalytic efficacy of ZrO_2. This imperative stems from the potential of ZrO_2 to play a pivotal role in advancing catalytic processes and unlocking its maximum activity warrants dedicated exploration. Relying solely on zirconia falls short due to its inadequate specific surface area, contributing to insufficient dispersion of active components. A groundbreaking advancement in the form of fibrous silica spheres, exemplified by KCC-1, has recently emerged as a result of the work by Polshettiwar, Cha [14]. This fibrous morphology possesses an extraordinary external area, an expansive open-pore framework, and remarkable thermal and hydrothermal stability. This achievement has sparked the interest of numerous researchers, propelling them to explore its application in CO methanation [15-18]. The endeavour to develop a fibrous silica-based catalyst boasting both micro- and mesoporosities and a substantial surface area carries the potential to dramatically enhance the catalytic capabilities of CO methanation. Furthermore, such a catalyst offers a promising platform for achieving a high dispersion of metal particles, fostering a synergistic interplay amongst the metal particles and the active support sites to amplify the efficacy of CO methanation. Building upon this precedent, the current study aims to explore into the efficacy of FSZr in the realm of CO methanation. This investigation seeks to further enrich our understanding of how FSZr can contribute to catalytic advancements in this domain.

2 Experimental

2.1 Material

Tetraethoxysilane (TEOS), hexadecyltrimethylammonium bromide (CTAB), 1-butanol, urea, and toluene were attained from Merck Sdn Bhd. Zirconia was purchased from Sigma-Aldrich.

2.2 Catalyst's Synthesis

Fibrous silica zirconia (FSZr) was synthesized through the hydrothermal technique. The process was initiated by dissolving both CTAB and urea in distilled water. A distinct blend containing TEOS, zirconia particulates, toluene, and 1-butanol was incorporated into this solution. The amalgamated solution was then uniformly stirred and heated to a temperature of 80 °C. Subsequent to cooling, the composite was desiccated prior to undergoing calcination at 550 °C for a duration of 6 hours. FSZr is composed of 10% ZrO_2, with SiO_2 constituting the primary constituent. The incorporation of ZrO_2 into a SiO_2 matrix may exert a negligible influence on the lattice of ZrO_2 owing to several underlying mechanisms. Both ZrO_2 and SiO_2 exhibit congruent crystal structures characterized by oxygen ions as the primary constituents, interspersed with metal cations at interstitial sites [19]. This structural similarity facilitates the seamless integration of silica within the zirconia lattice, mitigating pronounced lattice perturbations. Furthermore, ZrO_2 is typically introduced into a SiO_2 matrix in minor proportions, thereby predominantly eliciting a dilution effect. Consequently, the presence of ZrO_2 within the SiO_2 matrix may engender insignificant alterations in the overarching lattice parameters of the zirconia phase. For assessment purposes, commercially available ZrO_2 underwent calcination at 550 °C for a period of 6 hours.

2.3 Characterization

An array of instrumentation was employed to assess the physicochemical attributes of the synthesized material. The morphological features of the samples were scrutinized expending a field emission scanning electron microscope (FESEM) model JSM-6701F manufactured by JEOL. The crystalline phase characteristics of the catalyst were evaluated using the Bruker Advance D8 X-ray Diffraction equipment. Existing functional groups in the catalyst were investigated through Fourier transform infrared (FTIR) spectroscopy utilizing the PerkinElmer Inc. SPECTRUM GX FT-IR Microscope. For an in-depth analysis of the catalyst's basic properties, spectroscopic techniques employing pyrrole probing were employed. These investigations were conducted on-site utilizing the same FT-IR spectrometer. Preceding to investigation, all specimens underwent a one-hour activation process at 400 °C. The activated catalyst was then exposed to 0.533 kPa of pyrrole at ambient temperature for 15 minutes, succeeded by a 15-minute outgassing period. Each spectrogram was captured at ambient temperature by conducting three scans with a spectral resolution of 8 cm^{-1}. To assess the adsorption and desorption behaviors of nitrogen (N_2), SA 3100 W/L surface area and pore size analyzer by Beckman Coulter were utilized. The determination of the catalyst's surface area was accomplished using the Brunauer-Emmet-Teller (BET) surface area analysis technique. Additionally, the Barret-Joyner-Halenda (BJH) methodology was employed to measure the distribution of pore sizes within the catalyst.

2.4 Catalytic CO Methanation Evaluation

Catalytic CO methanation was carried out in a quartz fixed bed reactor with operating temperatures ranging from 200 to 500 °C. Preceding the commencement of the reaction, a quantity of 200 mg of catalyst underwent a sequence of preparatory procedures under a nitrogen stream for a duration of 30 minutes at a temperature of 550 °C to eliminate impurities. Subsequently, a flow of hydrogen was introduced for a duration of 2 hours at the

same temperature of 550 °C, thereby activating the catalyst. The catalyst was then allotted to chill to the targeted temperature, facilitated by a stream of nitrogen. After the temperature had reached a stabilized state, a gaseous feed mixture (comprising hydrogen and carbon monoxide) in a ratio of 3:1 was directed into the reactor. In order to eradicate any moisture from the final stream and enable easy entry into the gas chromatograph, a moisture trap was strategically positioned along the gas line exiting the system. The evaluation of product composition was conducted utilizing the 7820 Agilent gas chromatograph, which was outfitted with a thermal conductivity detector. Following a period of 10 minutes for each temperature setting to achieve stabilization, the resulting products were collected for the purpose of activity and selectivity assessment. CO conversion, CH_4 selectivity, CO_2 selectivity, and yield of CH_4 and CO_2 will all be computed using the formula below, respectively [Eq. (1-5)]:

$$X_{CO}\ (\%) = \frac{M_{CH_4} + M_{CO_2}}{M_{CO} + M_{CH_4} + M_{CO_2}} \times 100 \quad (1)$$

$$S_{CH_4}\ (\%) = \frac{M_{CH_4}}{M_{CH_4} + M_{CO_2}} \times 100 \quad (2)$$

$$S_{CO_2}\ (\%) = \frac{M_{CO_2}}{M_{CH_4} + M_{CO_2}} \times 100 \quad (3)$$

$$Y_{CH_4}\ (\%) = \frac{X_{CO} \times S_{CH_4}}{100} \quad (4)$$

$$Y_{CO_2}\ (\%) = \frac{X_{CO} \times S_{CO_2}}{100} \quad (5)$$

3 Result and Discussion

3.1 Characteristic Investigation

Fig. 1 depicts the morphological characteristics of FSZr, as revealed through FESEM investigation. FSZr displayed a distinctive structure marked by a porous and uniformly spherical arrangement, featuring a remarkable dendrimeric morphology. The particles showcased a consistent size range, spanning from 400 to 600 nm. These findings underscore the successful achievement of FSZr synthesis in a fibrous form. The spacing between each distinct dendrimer structure facilitated unobstructed diffusion of reactants, thereby fostering an environment conducive to achieving elevated levels of catalytic performance.

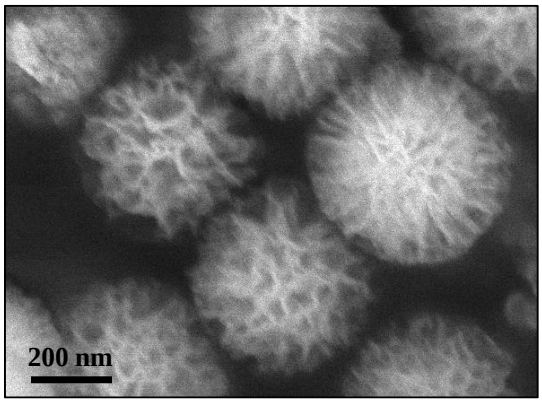

Fig. 1. FESEM image of FSZr

The XRD patterns of both FSZr and commercially available ZrO_2 are presented in Fig. 2, enabling the observation of their respective phases and crystalline architectures. Both catalysts exhibited a composition dominated by both the monoclinic (m-ZrO_2) and tetragonal (t-ZrO_2) states. The monoclinic phase of ZrO_2 (m-ZrO_2) was characterized by prominent principal peaks evident at 2θ values of 28.2°, 31.8°, and 41.0°, paralleling to the crystallographic planes (-111), (111), and (211), correspondingly. Additionally, the emergence of minor peaks at 2θ = 34.5°, indicative of the (110) planes, corroborated the presence of tetragonal ZrO_2 (t-ZrO_2) [20]. The distinctive diffraction patterns exhibited by the FSZr catalyst closely resemble ZrO_2, indicating that the inclusion of SiO_2 to the ZrO_2 matrix has negligible impact on the lattice assembly of ZrO_2. An individual, broad diffraction peak, situated at a 2θ angle of 22.8°, was identified. This peak corresponds to the existence of an amorphous SiO_2 form within the composition of the FSZr catalyst [21].

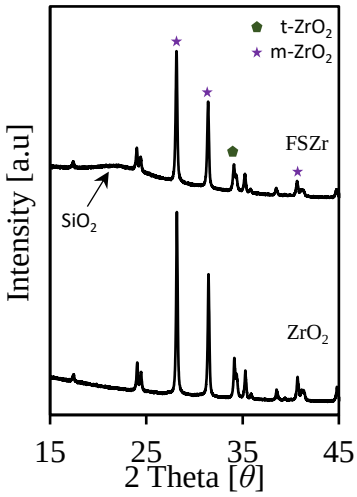

Fig. 2. XRD patterns of FSZr and ZrO_2

Fig. 3 exemplifies the N_2 physisorption isotherm and the pore size distribution profiles of FSZr and ZrO_2, correspondingly. The adsorption isotherm of the FSZr catalyst showcased characteristics attributed to type IV behavior, accompanied by an H3 hysteresis loop. These features are indicative of a mesoporous structure corresponding to the division established by the International Union of Pure and Applied Chemistry

(IUPAC) [22]. In contrast, the unmodified ZrO_2 displayed a type IV isotherm coupled with an H_2 hysteresis loop, which aligns with the anticipated behavior of mesoporous inorganic oxides [23]. The specific surface area measurements for FSZr and ZrO_2 were determined as 450.6 and 8.7 m² g^-1, respectively. In terms of pore dimensions, the FSZr samples exhibited a wide and prominent peak within the mesoporous range spanning from 1 to 5 nm. Conversely, ZrO_2 displayed a distinct peak at around 2 nm. Notably, the peak attributed to FSZr was significantly more pronounced and broader in comparison to the ZrO_2 peak. This observation implies that the FSZr catalyst possesses a notably greater mesoporous volume, consequently yielding a larger surface area in contrast to ZrO_2.

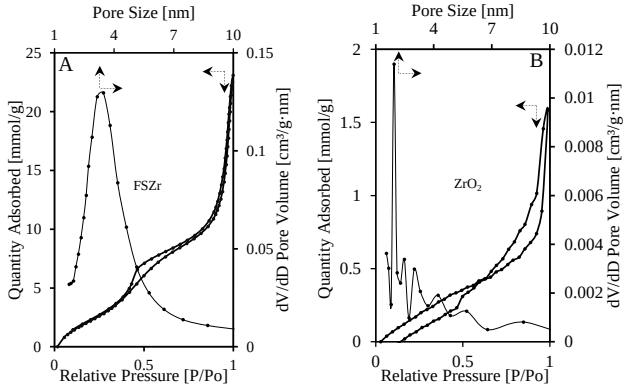

Fig. 3. N_2 physisorption isotherm of (A) FSZr and (B) ZrO_2.

FTIR spectroscopy stands as a notably efficacious methodology for acquiring vibrational insights pertaining to species inherent within materials. The outcomes of the FTIR analysis, conducted using potassium bromide (KBr) as a medium, are visually depicted in Figure 4 for both FSZr and ZrO_2. In the case of FSZr, a series of absorption bands were discerned at wavenumbers of 472 cm^{-1}, 802 cm^{-1}, 970 cm^{-1}, and 1091 cm^{-1}, concurring with the vibrational characteristics accredited to Si-O-Si bending, Si-O-Si symmetrical stretching, the overlap of Si–O–Zr and the external manifestation of Si–OH groups, in addition to the asymmetric stretching of Si-O-Si bonds, respectively [24, 25].

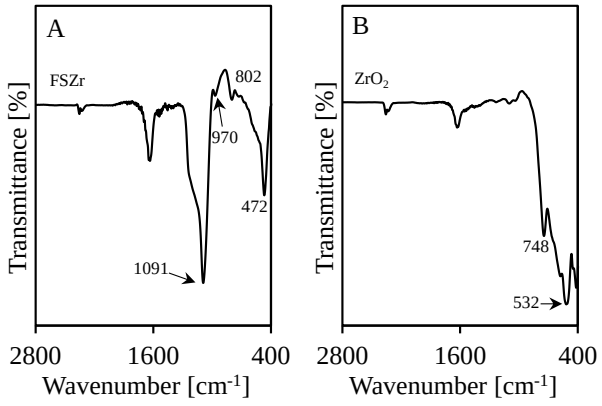

Fig. 4. FTIR spectra (A) FSZr and (B) ZrO_2

The existence of these spectral bands serves to validate the emergence of the mesoporous structure. In contrast, ZrO_2 manifests diverse absorption bands, notably including those attributed to monoclinic Zr-O vibrations at 750 cm^{-1} and ZrO_2 skeletal vibrations at 534 cm^{-1}. Within the FSZr sample, conspicuous indications are presented by Si–O–Zr linkages that coincide with the presence of external Si–OH groups. This phenomenon suggests the substitution of hydrogen in the Si–OH entities by zirconium ions, thereby engendering a distinct set of Si–O–Zr bonds [20].

The inherent basicity and its potency of all catalysts were evaluated using pyrrole adsorption FTIR, as illustrated in Fig. 5. Within the spectral range of 3600 to 3000 cm^{-1}, there were noticeable signals associated to the altered stretching of N-H bonds in the pyrrole molecule (C_4H_4NH) observed in all catalysts. These signals indicate interactions between pyrrole and the basic sites within the catalyst's structure, specifically at the oxygen sites [15]. A rise in the concentration of basic sites correlated with greater peak area and strength. Remarkably, FSZr displayed the most prominent peak strength, implying the existence of the highest basic sites concentration. Crucially, the strength of basicity aligned with the efficiency of CO methanation, with stronger basicity resulting in enhanced CO methanation performance. This phenomenon can be attributed to the tendency of acidic carbon oxide gases to gravitate toward basic regions due to their attractive properties. Consequently, augmenting the level of basicity results in enhanced CO adsorption capabilities.

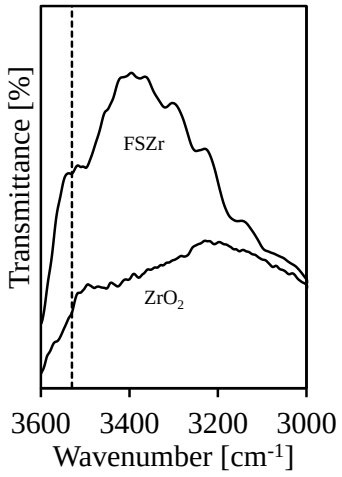

Fig. 5. Pyrrole-adsorbed FTIR spectra of FSZr and ZrO_2

3.2 CO Methanation Performance

An investigation into the catalytic capability of the catalyst in the context of the CO methanation process utilizing a stable reactor were conducted. The study encompassed temperatures varying from 200°C to 500°C, and the atmospheric pressure was maintained at a constant level throughout the experiment. Fig. 6 provides a visual representation of how the catalyst performed in terms of converting CO and producing CH_4 within the CO methanation reaction.

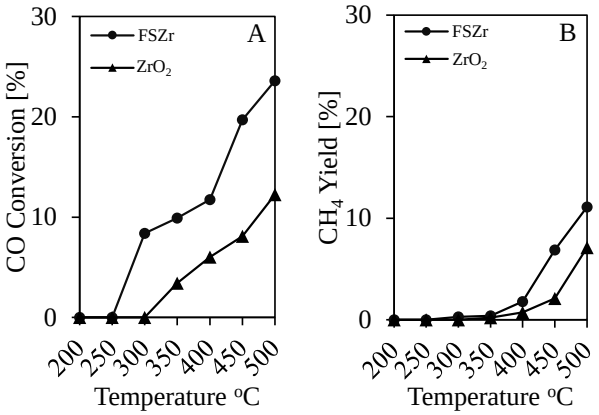

Fig. 6. (A) CO conversion and (B) CH_4 yield of FSZr and ZrO_2 catalysts for CO methanation.

It was observed that FSZr exhibited superior performance compared to ZrO_2 concerning the CO conversion and CH_4 yield in the context of CO methanation activity. FSZr displayed initiation of activation at 250 °C, which underwent gradual enhancement with the rise in reaction temperature within the 250 to 500 °C range. On the other hand, ZrO_2 demonstrated its activation at a slightly higher temperature of 300 °C. Taking into consideration the exothermic nature of the CO methanation, thermodynamically lower temperatures are favorable; however, they suffer from compromised kinetics due to sluggish reaction rates. Consequently, elevated temperatures are imperative to attain notable CO conversion and CH_4 selectivity. At 500 °C, FSZr exhibited noteworthy capability with a CO conversion rate of 23.58% and CH_4 yield of 11.10%, surpassing ZrO_2. This outcome underscores the efficacy of the FSZr catalyst in enhancing CO methanation activity. Furthermore, it's noteworthy that the sequence of performance aligned with the catalyst's surface area and basicity. Higher surface area and basicity correlated with augmented CO methanation efficiency. This observation underscores the substantial impact of surface area and basicity on the achieved exceptional performance, as larger surface areas facilitated enhanced accessibility to active sites, while heightened basicity contributed to superior reactant adsorption capability.

4 Conclusion

In summary, the successful synthesis of fibrous silica zirconia through hydrothermal means has been achieved, followed by its effective utilization in carbon monoxide methanation. Morphological investigation via FESEM revealed a distinctive spherical configuration resembling cockscombs, characterized by dendrimeric fibers within the FSZr, ranging in size from 400 to 600 nm. The XRD pattern attests to the successful incorporation of ZrO_2 onto the FSZr catalyst's surface. Furthermore, FSZr exhibited markedly superior attributes in terms of surface area and pore volume when contrasted with ZrO_2. The fibrous morphology, coupled with the augmented surface area, has been instrumental in conferring superior performance upon FSZr in comparison to the ZrO_2 catalyst. These influences play a pivotal role in expanding the active sites for adsorption of hydrogen and carbon monoxide, consequently augmenting the catalytic efficiency. The significance of this study extends to its potential in advancing comprehension regarding the intricate interplay amongst fibrous morphology and zirconia within CO methanation. This comprehension bears the promise of contributing towards meeting the global energy demand in a more effective manner.

This investigation was funded by the Universiti Teknologi Malaysia's UTM Fundamental Research (UTMFR) with Grant No. 22H51.

References

1. S. Ronsch, J. Schneider, S. Matthischke, M. Schluter, M. Gotz, J. Lefebvre, P. Prabhakaran, and S. Bajohr, Review on methanation - From fundamentals to current projects. Fuel. **166**, 276-296 (2016)
2. H. Wang, Y. Pei, M. Qiao, and B. Zong, Advances in methanation catalysis. **29**, 1-28 (2017)
3. A.H. Hatta, A.A. Jalil, N.S. Hassan, M.Y.S. Hamid, A.F.A. Rahman, L.P. Teh, and D. Prasetyoko, A review on recent bimetallic catalyst development for synthetic natural gas production via CO methanation. Int J Hydrogen Energ. **47**, 30981-31002 (2022)
4. A.H. Hatta, A.A. Jalil, N.S. Hassan, M.Y.S. Hamid, W. Nabgan, M. Alhassan, M.B. Bahari, C.K. Cheng, S.H. Zein, and M.L. Firmansyah, A short review on informetric analysis and recent progress on contribution of ceria in Ni-based catalysts for enhanced catalytic CO methanation. Powder Technol. 118246 (2023).
5. A. Safari, N. Das, O. Langhelle, J. Roy, and M. Assadi, Natural gas: A transition fuel for sustainable energy system transformation? Energy Science & Engineering. **7**, 1075-1094 (2019)
6. J. Kopyscinski, T.J. Schildhauer, and S.M.A. Biollaz, Production of synthetic natural gas (SNG) from coal and dry biomass - A technology review from 1950 to 2009. Fuel. **89**, 1763-1783 (2010)
7. I. Hussain, A.A. Jalil, N.A.A. Fatah, M.Y.S. Hamid, M. Ibrahim, M.A.A. Aziz, and H.D. Setiabudi, A highly competitive system for CO methanation over an active metal-free fibrous silica mordenite via in-situ ESR and FTIR studies. Energy Convers. Manage. **211**, (2020)
8. B. Miao, S.S.K. Ma, X. Wang, H.B. Su, and S.H. Chan, Catalysis mechanisms of CO_2 and CO methanation. Catal Sci Technol. **6**, 4048-4058 (2016)
9. I. Hussain, A.A. Jalil, N.S. Hassan, M. Farooq, M.A. Mujtaba, M.Y.S. Hamid, H.M.A. Sharif, W. Nabgan, M.A.H. Aziz, and A.H.K. Owgi, Contemporary thrust and emerging prospects of

catalytic systems for substitute natural gas production by CO methanation. Fuel. **311**, (2022)
10. A.H. Chen, T. Miyao, K. Higashiyama, and M. Watanabe, High catalytic performance of mesoporous zirconia supported nickel catalysts for selective CO methanation. Catal Sci Technol. **4**, 2508-2511 (2014)
11. Q. Guo, S.Z. Li, J. Li, Y.K. Hu, and Y.X. Li, Effect of SiO_2 on the CO Selective Methanation over SiO_2/Ni-ZrO_2 Catalysts. Chemcatchem. **14**, (2022)
12. H.L. Lu, X.Z. Yang, G.J. Gao, K.B. Wang, Q.Q. Shi, J. Wang, C.H. Han, J. Liu, M. Tong, X.Y. Liang, and C.F. Li, Mesoporous zirconia-modified clays supported nickel catalysts for CO and CO_2 methanation. Int J Hydrogen Energ. **39**, 18894-18907 (2014)
13. L. Zhang, Z.M. Gao, L.X. Bao, and H.W. Ma, Influence of the supports ZrO_2 on selective methanation of CO over the nickel supported catalysts. Int J Hydrogen Energ. **43**, 9287-9295 (2018)
14. V. Polshettiwar, D. Cha, X.X. Zhang, and J.M. Basset, High-Surface-Area Silica Nanospheres (KCC-1) with a Fibrous Morphology. Angew Chem Int Edit. **49**, 9652-9656 (2010)
15. N.A.A. Fatah, A.A. Jalil, S. Triwahyono, N. Yusof, C.R. Mamat, S.M. Izan, M.Y.S. Hamid, I. Hussain, R.H. Adnan, T.A.T. Abdullah, and W. Nabgan, Favored hydrogenation of linear carbon monoxide over cobalt loaded on fibrous silica KCC-1. Int J Hydrogen Energ. **45**, 9522-9534 (2020)
16. A.H. Hatta, A.A. Jalil, M.Y.S. Hamid, N.S. Hassan, I. Hussain, and N.W.C. Jusoh, The interparticle oxygen vacancies enrichment in the matrix of fibrous silica ceria supported nickel for CO methanation. Fuel. **333**, (2023)
17. I. Hussain, A.A. Jalil, C.R. Mamat, T.J. Siang, A.F.A. Rahman, M.S. Azami, and R.H. Adnan, New insights on the effect of the H_2/CO ratio for enhancement of CO methanation over metal-free fibrous silica ZSM-5: Thermodynamic and mechanistic studies. Energy Convers Manag. **199**, (2019)
18. L.P. Teh, S. Triwahyono, A.A. Jalil, M.L. Firmansyah, C.R. Mamat, and Z.A. Majid, Fibrous silica mesoporous ZSM-5 for carbon monoxide methanation. Appl Catal A-Gen. **523** 200-208 (2016) ,
19. Y.-y. Ma, P.-n. Jia, X.-c. Li, N. Liu, and Y.-l. Ma, Synthesis of the ZrO_2–SiO_2 microspheres as a mesoporous candidate material. J. Porous Mater. **19**, 1047-1052 (2012)
20. F.F.A. Aziz, A.A. Jalil, N.S. Hassan, C.N.C. Hitam, A.F.A. Rahman, and A.A. Fauzi, Enhanced visible-light driven multi-photoredox Cr(VI) and p-cresol by Si and Zr interplay in fibrous silica-zirconia. J Hazard Mater. **401**, 123277 (2021)
21. M.Y.S. Hamid, M.L. Firmansyah, S. Triwahyono, A.A. Jalil, R.R. Mukti, E. Febriyanti, V. Suendo, H.D. Setiabudi, M. Mohamed, and W. Nabgan, Oxygen vacancy-rich mesoporous silica KCC-1 for CO_2 methanation. Appl Catal A-Gen. **532**, 86-94 (2017)
22. N.F. Khusnun, A.A. Jalil, S. Triwahyono, N.W.C. Jusoh, A. Johari, and K. Kidam, Interaction between copper and carbon nanotubes triggers their mutual role in the enhanced photodegradation of p-chloroaniline. Phys Chem Chem Phys. **18**, 12323-12331 (2016)
23. N.J. Abd Rahman, A. Ramli, K. Jumbri, and Y. Uemura, Tailoring the surface area and the acid-base properties of ZrO_2 for biodiesel production from Nannochloropsis sp. Sci Rep-Uk. **9**, 16223 (2019)
24. N.S. Hassan, A.A. Jalil, C.N.C. Hitam, M.H. Sawal, M.N.S. Rahim, I. Hussain, N.W.C. Jusoh, R. Saravanan, and D. Prasetyoko, Enhanced photooxidative desulphurization of dibenzothiophene over fibrous silica tantalum: Influence of metal-disturbance electronic band structure. Int J Hydrogen Energ. **48**, 6575-6585 (2022)
25. A.H. Hatta, A.A. Jalil, M.Y.S. Hamid, N.S. Hassan, I. Hussain, and N.W.C. Jusoh, The interparticle oxygen vacancies enrichment in the matrix of fibrous silica ceria supported nickel for CO methanation. Fuel. **333**, 126539 (2023)